Title

The potential value of probabilistic tractography-based for MR-guided focused ultrasound thalamotomy for essential tremor

Authors

Tsolaki, Evangelia
Downes, Angela
Speier, William
et al.

Publication Date

2018

DOI

10.1016/j.nicl.2017.12.018

Peer reviewed

NeuroImage: Clinical 17 (2018) 1019–1027

Contents lists available at ScienceDirect

NeuroImage: Clinical

journal homepage: www.elsevier.com/locate/ynicl

The potential value of probabilistic tractography-based for MR-guided focused ultrasound thalamotomy for essential tremor

Evangelia Tsolaki[a,*], Angela Downes[a], William Speier[a], W. Jeff Elias[b], Nader Pouratian[a,c]

[a] Department of Neurosurgery David Geffen School of Medicine, UCLA, Los Angeles, CA, USA
[b] Department of Neurosurgery, University of Virginia, Charlottesville, VA, USA
[c] Brain Research Institute David Geffen School of Medicine, UCLA, Los Angeles, CA, USA

ARTICLE INFO

Keywords:
Magnetic resonance imaging-guided focused ultrasound
Tremor
Tractography

ABSTRACT

Magnetic Resonance-guided Focused UltraSound (MRgFUS) offers an incisionless approach to treat essential tremor (ET). Due to lack of evident internal anatomy on traditional structural imaging, indirect targeting must still be used to localize the lesion. Here, we investigate the potential predictive value of probabilistic tractography guided thalamic targeting by defining how tractography-defined targets, lesion size and location, and clinical outcomes interrelate.

MR imaging and clinical outcomes from 12 ET patients that underwent MRgFUS thalamotomy in a pilot study at the University of Virginia were evaluated in this analysis. FSL was used to evaluate each patient's voxel-wise thalamic connectivity with FreeSurfer generated pre- and post-central gyrus targets, to generate thalamic target maps. Using Receiver Operating Characteristic curves, the overlap between these thalamic target maps and the MRgFUS lesion was systematically evaluated relative to clinical outcome. To further define the connectivity characteristics of effective MRgFUS thalamotomy lesions, we evaluated whole brain probabilistic tractography of lesions (using post-treatment imaging to define the lesion pre-treatment diffusion tensor MRI). The structural connectivity difference was explored between subjects with the best clinical outcome relative to all others.

Ten of twelve patients presented high percentage of overlapping between connectivity-based thalamic segmentation maps and lesion area. The improvement of clinical score was predicted (AUC: 0.80) using the volume of intersection between the thalamic target (precentral gyrus) map and MRgFUS induced lesion as feature. The main structural differences between those with different magnitudes of response were observed in connectivity to the pre- and post-central gyri and brainstem/cerebellum.

MRgFUS thalamotomy lesions characterized by strong structural connectivity to precentral gyrus demonstrated better responses in a cohort of patients treated with MRgFUS for ET. The intersection between lesion and thalamic-connectivity maps to motor - sensory targets proved to be effective in predicting the response to the therapy. These imaging techniques can be used to increase the efficacy and consistency of outcomes with MRgFUS and potentially shorten treatment times by identifying optimal targets in advance of treatment.

1. Introduction

Essential tremor (ET) is the most common movement disorder in adults (Li SC SB et al., 1985; Louis and Ferreira, 2010) with significant impact on patients' abilities to perform daily activities (Chandran and Pal, 2013). Abnormal activity of central tremor network is considered as a cause (Brittain et al., 2015; Raethjen and Deuschl, 2012) although the precise pathogenesis remains incompletely understood (Elias and Shah, 2014; Louis, 2014). Transcranial high intensity Magnetic Resonance-guided Focused UltraSound (MRgFUS) targeting the ventral intermediate nucleus of the thalamus (Vim) is a significant development in the field of functional neurosurgery that offers an incisionless approach to treat ET. It creates thermal lesions through an intact skull with immediate results with the ability to assess the patient for both therapeutic benefit and side effects between sonications. The efficacy of MRgFUS for treating ET has been reported both in smaller institutional series (Elias et al., 2013; Lipsman et al., 2013) as well as a larger randomized clinical trial (Elias et al., 2016).

The VIM nucleus is approximately $4 \times 4 \times 6\ mm^3$ in size (Louis and Ottman, 1998) and anatomically has been described as the cerebellar receiving area of the thalamus before the fibers project to the motor cortices (Fang et al., 2016; Hyam et al., 2012; Ilinsky and Kultas-

* Corresponding author at: Department of Neurosurgery, University of California, Los Angeles, 300 Stein Plaza, Suite 562, Los Angeles, CA 90095, USA.
E-mail address: etsolaki@mednet.ucla.edu (E. Tsolaki).

https://doi.org/10.1016/j.nicl.2017.12.018
Received 3 August 2017; Received in revised form 8 December 2017; Accepted 9 December 2017
Available online 12 December 2017

Ilinsky, 2002), although it is incompletely defined from a connectivity standpoint and cerebellothalamic fibers are likely not absolutely unique to the ViM nucleus. Indirect targeting is the most common method to define the location of Vim. Atlas-derived coordinates are superimposed onto a patient's unique magnetic resonance imaging (MRI) scan and stereotactic coordinates are defined in relation to a point on the anterior commissure – posterior commissure (AC-PC) line (Alusi et al., 2001; Bittar et al., 2005; Dormont et al., 1997). The precise targeting of VIM is crucial for successful surgical intervention and is associated with improved surgical outcomes (Papavassiliou et al., 2004). The limitations of indirect targeting using atlas-based coordinates have long been recognized due to the limited data set on which atlases are created and extensive interpatient anatomical and functional variability (Nowinski et al., 2006, 2004; O'Gorman et al., 2011).

Diffusion tensor imaging (DTI) is a non-invasive technique that has been used to delineate the internal anatomy of the thalamus by tracing white matter tracts to cortical areas and cerebellum that are involved in tremor (Coenen et al., 2011; Hyam et al., 2012; Kim et al., 2017; Kincses et al., 2012; Klein et al., 2012; Pouratian et al., 2011; Sammartino et al., 2016). Probabilistic tractography takes into account intra-voxel crossing fibers (Behrens et al., 2003a), estimates the pathways that originate at any given seed voxel and provides quantitative information about the probability of structural connectivity that a white matter tract will pass through any other voxel in the brain (Behrens et al., 2003b). Individualized DTI segmentation tractography may provide more robust anatomic data for targeting thalamic nuclei and it has the potential to guide and refine thalamic targeting for improved efficacy in thalamotomies and reduced number of adverse events. In this study, we used retrospective imaging data from ET patients that underwent MRgFUS from the initial pilot trial reported by Elias et al., (2013). We hypothesize that the efficacious target area is localized within the part of the thalamus with the highest probability of connectivity with precentral gyrus, which contains premotor and primary motor cortices, since it plays an important role in tremor generation (Pouratian et al., 2011). Our goal is to understand the predictive value of probabilistic tractography guided thalamic targeting by defining how tractography-defined targets, lesion size, location and clinical outcomes interrelate.

2. Methods

2.1. Patients

Twelve patients with refractory essential who were treated with MRgFUS targeting Vim in a pilot study at the University of Virginia (Elias et al., 2013) were evaluated in this analysis, for whom pre-operative DTI sequences were available. All patients provided written informed consent. Details of MRgFUS procedure (including sonication, maximum temperature, and other clinical variables) have been described previously (Elias et al., 2013). Briefly, an MRI–guided focused ultrasound system (ExAblate Neuro, InSightec) was used to deliver therapeutic sonication to each patient targeting Vim contralateral to the affected hand. The Vim location was specified pre-operatively as three quarters of the length of the anterior-posterior commissural line and 14 to 15 mm lateral to the midline or 11 mm lateral to third ventricle. For each patient, Vim localization was adjusted further intraoperatively based on the suppression of tremor that each patient presented.

2.2. Clinical assessment

As described at (Elias et al., 2013), Clinical Rating Scale for Tremor (CRTS) (Stacy et al., 2007) was used for the clinical evaluation pre-treatment and 1 week, 1 month, 3 months and 12 months after MRgFUS treatment. Different components of CRTS were used to evaluate the tremor severity, the ability to perform tasks and functional disability of the patients. In current study, we use the tremor severity component to assess each patient's condition at different time points in a range of 0 to 32, with higher scores indicating high tremor severity. As described below, given the overall favorable response across all subjects, we leveraged differences in outcomes even amongst those with favorable outcomes by dividing the group into 2, which we refer to as those with “superior” and “inferior outcomes.” To be clear, “inferior outcomes is not meant to imply “non-responder” but was a method used to compare across 2 groups.

2.3. Image acquisition

For current study, T1-and T2- weighted and diffusion-weighted MR data, acquired at University of Virginia before and 1 month after treatment, were used. A 3 Tesla MRI scanner with 8-channel head array coil (Tim Trio, Siemens Medical Solutions, Germany) was used. A 2D twice-refocused DW-SE-EPI sequence was used for DTI acquisition. Diffusion tensor imaging parameters were: field of view 230 × 230; b value = 1000 s/mm^2; 20 directions; number of slices = 30; matrix size = 128 × 128; repetition time/echo time = 4100/93 ms. High resolution structural images were collected using 3D MP-Rage sequence with the following parameters: repetition time/echo time/inversion time = 1900/1.94/900 ms; a flip angle of 9°; number of slices = 240; matrix = 256 × 256.

2.4. Regions of interest

FreeSurfer (version 5.3.0, http://surfer.nmr.mgh.harvard.edu/) was used for cortical surface reconstruction and volumetric segmentation to automatically generate thalamic as well as pre- and post-central gyrus regions of interest (ROIs) on pre-treatment T1-weighted images for each patient. The MRgFUs treatment-induced lesion area was delineated on 1 month post-operative T2-weighted image registered to pre-treatment T1-weighted image (Fig. 1a, b, c). Specifically, the lesion was localized and then the maximum intensity value of the area around the localization point was retrieved. Based on the imaging findings previously reported (Elias et al., 2013; Wintermark et al., 2014), 1 month after MRgFUS treatment the lesion consisted of 3 concentric zones with different diameters. In order to localize the center of the lesion, we used as upper threshold the maximum intensity value and as lower the 60% of the maximum intensity of the selected area and then the lesion was drawn manually for each subject. To register the ROIs and lesion area to preoperative DTI space, linear and non-linear transformations (FLIRT-FNIRT) (Andersson et al., 2007; Jenkinson et al., 2002) were performed to register pretreatment T1 and DTI to MNI152 template (using mutual information as cost function, 6 degrees of freedom for DTI to T1 registration and 12 for registration to MNI152) and the derived transformation matrices were used for the transformation.

2.5. Tractography analysis

Probabilistic diffusion tractography was performed to define structural connectivity between the thalamus with pre- and post-central gyrus ROIs using the FMRIB's Diffusion toolbox. Eddy current correction was used to apply affine registrations to each volume in the diffusion dataset to register it with the initial reference B0 volume prior performing tractography. Skull stripping was performed using the brain extraction tool (BET) (Smith, 2002). A multi-fiber diffusion model in FDT (Behrens et al., 2003b) was fitted on the data. This model uses Bayesian techniques to estimate a probability distribution function (PDF) on the principal fiber direction at each voxel, accounting for the possibility of crossing fibers within each voxel. Two fibers modeled per voxel, a multiplicative factor (i.e., weight) of 1 for the prior on the additional modeled fibers, and 1000 iterations before sampling (Behrens et al., 2007). Using these PDFs and PROBTRACKX, we could then determine the probability of connectivity between thalamus and the pre- and post-central gyrus targets. From each voxel in the thalamic

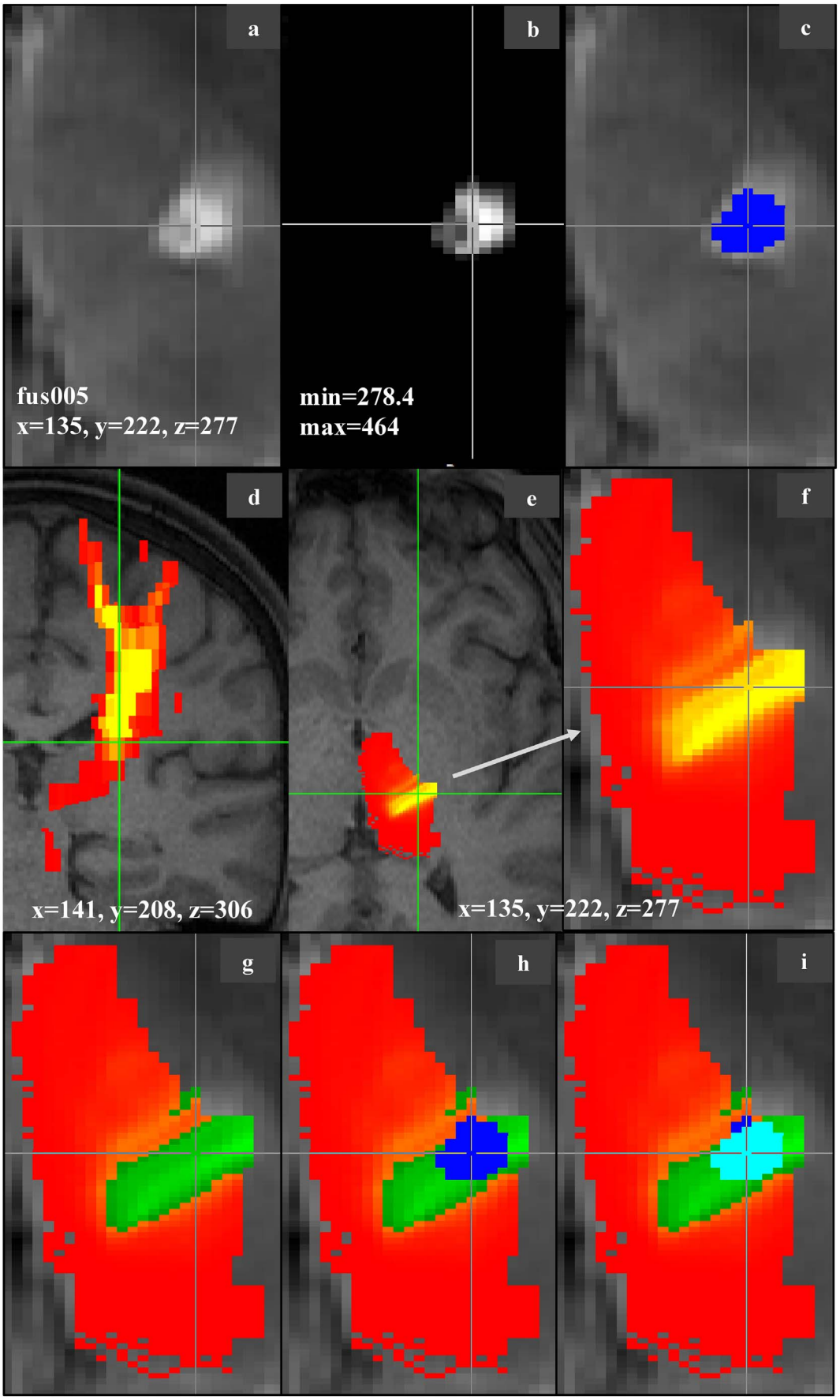

(caption on next page)

Fig. 1. Localization of MRgFUs treatment-induced lesion area and calculation of intersection area between lesion and thalamic probabilistic maps.
a) At T2-weighted image registered to pre-treatment T1-weighted image the MRgFUs treatment-induced lesion area was localized and (b) based on the maximum intensity value of the lesion area (upper threshold: maximum intensity value - lower a percentage of 60% of the maximum intensity value), (c) the lesion was delineated (blue color). d) Fiber tract projections from the thalamic region with maximal connectivity with to the target (precentral gyrus in this case) were derived. e) Connectivity-based thalamic segmentation map (red-yellow map) to pre-central gyrus were found (zoom out (f)). (g) Segmentation map was thresholded at 30% of the maximum intensity value (green map) to find the voxels with high probability of connectivity to target area. (h) The lesion area was overlapped with the thalamic segmentation map and the intersection was calculated (light blue) (i).

seed, 5000 streamlines were generated; a 0.2 curvature threshold was chosen, a loop check termination was used and the target masks were used as waypoint, termination and classification masks. The resulted tomographic probabilistic maps identified the regions within thalamus with the highest probability of connectivity with pre- and post-central gyrus ROIs (Fig. 1e–f).

The same parameters were used using the lesion itself as a seed in order to investigate the structural connectivity of MRgFUs treatment-induced lesion area with the whole brain. Five thousand samples per voxel were again generated from each patient's lesion seed to whole brain using the cerebrospinal fluid as an exclusion mask. Each patient's whole brain tractography map was divided by the overall number of streamlines and then binarized at 0.05 threshold value.

Based on the clinical score 1 month and 1 year after MRgFUS 11 of the 12 patients and 10 of 12 patients demonstrated improvement greater that 50%, respectively. Given the overall response to therapy was satisfactory across the majority of subjects, we leveraged the differential degrees of response, even amongst “responders.” We used the median value of clinical improvement (0.84) to divide patients in two groups: one including the subjects with superior clinical outcome (n = 6, clinical improvement greater or equal to 0.84) and one with inferior (n = 6, clinical improvement < 0.84)). Notably, “inferior outcomes” is not meant to imply “non-responders.” The same approach was followed using the improvement in clinical score 1 year after MRgFUS and a cutoff value of 0.82 was used to label patients. Subjects that presented superior clinical outcome 1 month after MRgFUS had the same label also after 1 year (Table 1). The ‘common population map’ was found by summing up all the binarized maps and identifying those voxels in the whole brain that were shared by at least 80% of the subjects. Finally, the percentage of improvement in clinical score between baseline and 1 month and 1 year after MRgFUs was assigned to each subject's binary whole brain map. These clinically-weighted maps were then averaged to find the ‘average clinical efficacy map’ at the two timepoints for the 12 patients. Each voxel's value in the ‘average clinical efficacy map’ corresponds to the average clinical outcome of the subjects that present connectivity to that specific voxel.

Table 1
Characterization of patients using clinical improvement score 1 month and 1 year after MRgFUS.

Patients	Clinical score			1 m clinical improvement	1 y clinical improvement
	Treated hand	1 m	1y	Cutoff: 0.84	Cutoff: 0.82
fus001	20	3	3	0.85	0.85
fus002	22	6	8	0.73	0.64
fus004	29	6	6	0.79	0.79
fus005	20	0	0	1.00	1.00
fus006	16	0	2	1.00	0.88
fus008	15	8	11	0.47	0.27
fus009	24	4	5	0.83	0.79
fus0010	19	3	1	0.84	0.95
fus0011	28	10	17	0.64	0.39
fus0012	21	8	10	0.62	0.52
fus0013	14	0	2	1.00	0.86
fus0015	18	0	2	1.00	0.89

The median value 0.84 of the improvement in clinical score 1 month (m) after MRgFUS was used as cutoff value to divide patients in two groups: one including the subjects with superior clinical outcome (n = 6) and one with inferior (n = 6). The same approach was followed using the improvement in clinical score 1 year (y) after MRgFUS and the median value of 0.82 was used as cutoff to label patients. Subjects that characterized with superior clinical outcome 1 month after MRgFUS presented superior outcome also after 1 year.

2.6. Predictive value of the intersection between MRgFUS treatment-induced lesion and thalamic probabilistic maps

For each subject, the maximum intensity value within each thalamic probability map (based on connectivity to pre- and post-central gyri) was determined. As the optimal threshold is unknown and we aimed to understand how best to apply probabilistic tractography to define thalamic targets, thresholds for each map were applied at 30% (Fig. 1g), 40% and 50% of this maximum value in order to identify the voxels within the thalamic probabilistic maps with the higher probability of connectivity to pre- and post-central gyri. The percentage overlap between the MRgFUs treatment-induced lesion and each probabilistic map at each threshold (and also without threshold) was derived. Also, the volume of MRgFUS lesion (Fig. 1c) and segmentation maps (Fig. 1f, g) were compared to the overlapping volume (Fig. 1h). As an initial assessment, we evaluated whether lesion volume relates to response. We then investigated the predictive value of probabilistic tractography guided thalamic targeting by defining how tractography-defined targets, lesion size and location, and clinical outcomes interrelate. We used empirical receiver operating characteristic (ROC) curves to examine the sensitivity and specificity at all possible cutoffs (Park et al., 2004) of the overlapping.

3. Results

3.1. MRgFUS treatment-induced lesion structural connectivity

We evaluated whole brain probabilistic tractography seeded from the MRgFUS lesion (Fig. 2). The main differences between those with superior vs inferior clinical outcomes were located in connectivity to the pre- and post- central gyri as well as the brainstem/cerebellum (Fig. 2, green illustrates differences between groups). Superior clinical outcome was related to more dominant structural connectivity to both pre- and post- central gyrus and to the brainstem/cerebellum areas while inferior outcome was characterized by weak caudal projections to the cerebellum and precentral gyrus.

Likewise, the clinical efficacy map demonstrates that patients with higher clinical improvement 1 month and 1 year after MRgFUS present stronger structural connectivity to the pre- and post-central gyri and to the caudal projection to the cerebellum. (Fig. 3).

3.2. Overlapping volume between MRgFUS treatment-induced lesion and thalamic segmentation maps

The overlap between the connectivity-based thalamic segmentation maps to each cortical region (red-yellow maps on Fig. 1) and lesion area (blue mask on Fig. 1) was evaluated. The average lesion volume was found 111 ± 26 mm^3 and further investigation of the overlapping volume included only the area within thalamic segmentation probabilistic maps that characterized by higher probability of connectivity to target areas (green maps on Fig. 1) at different thresholds. Given the small size of data, we report all the raw data on Table 2.

For each patient, the voxels and the volume (VOL) of the MRgFUS induced lesion and of each thalamic segmentation map to pre-central (a) and post-central gyrus (b) were found. Also for each thalamic map

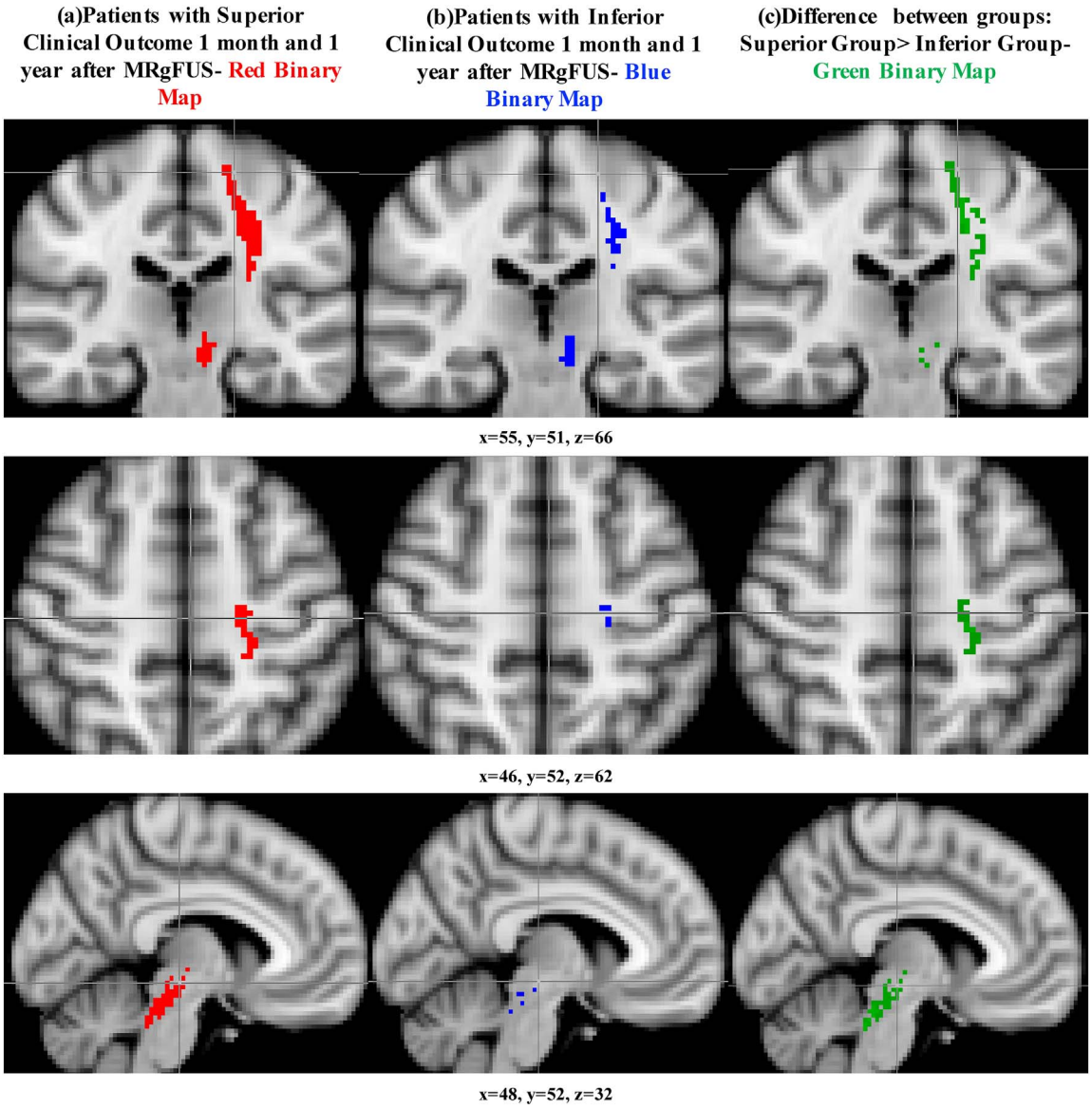

Fig. 2. Whole brain probabilistic tractography of shared fiber tract of MRgFUS induced lesion area.
Tractography from the MRgFUS lesion demonstrates that patients with (a) superior clinical outcome (n = 6) (red common whole brain binary map) present stronger structural connectivity than patients with (b) inferior clinical outcome (n = 6) (blue common whole brain binary map) in pre- and post-central gyri and brainstem/cerebellum areas. The differences (c) between the common whole brain binary map of the two groups were localized in pre- and post-central gyri (green binary map) and to the caudal projection to the cerebellum (green binary map).

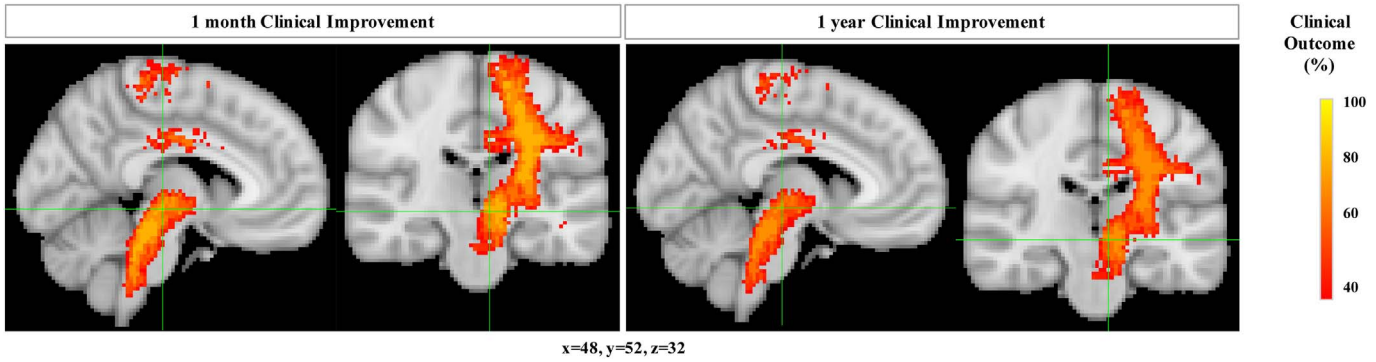

Fig. 3. Average clinical efficacy map using clinical improvement scores 1 month and 1 year after MRgFUS.
The percentage of improvement in clinical score between baseline and 1 month and 1 year after MRgFUs was assigned to each subject's binary whole brain map. The resulted clinically-weighted maps were then averaged to find the 'average clinical efficacy map' at two time points. Each voxel's value in the 'average clinical efficacy map' corresponds to the average clinical outcome of the subjects that present connectivity to that specific voxel. In both time points the patients with higher clinical improvement present stronger connectivity to pre- and post-central gyri and brainstem/cerebellum areas (Red-Yellow map).

Table 2
Overlapping volume between MRgFUS treatment-induced lesion and thalamic segmentation maps.

a) Thalamic segmentation map to precentral gyrus

	Lesion		TSM	VOL_O(mm^3)								(VOL_O/VOL_L)%				(VOL_O/VOL_TSM)%			
	V	VOL(mm^3)	V	MI	NT	30%	40%	50%	NT	30%	40%	50%	NT		40%	50%	NT	30%	40%	50%
fus001	430	103	28,587	4060	6816	693	585	505	103	68	59	52	100	66	57	50	1.51	9.81	10.09	10.30
fus002	292	70	24,929	3914	5944	1361	973	589	21	21	11	6	30	30	16	9	0.35	1.54	1.13	1.02
fus004	667	121	28,466	4381	5170	313	187	102	108	45	27	15	89	37	22	12	2.09	14.38	14.44	14.71
fus005	565	103	40,911	4580	7430	757	609	493	101	88	82	73	98	85	80	71	1.36	11.62	13.46	14.81
fus006	686	125	37,426	3903	6797	1274	1095	927	77	65	57	41	62	52	46	33	1.13	5.10	5.21	4.42
fus008	528	126	29,770	3758	7098	1025	848	688	126	126	125	123	100	100	99	98	1.78	12.29	14.74	17.88
fus009	377	90	32,749	4503	7808	1395	1234	1095	36	36	36	36	40	40	40	40	0.46	2.58	2.92	3.29
fus0010	694	126	37,783	4101	6862	750	608	479	80	57	48	38	63	45	38	30	1.17	7.60	7.89	7.93
fus0011	450	107	29,472	4225	7027	784	671	560	98	38	30	22	92	36	28	21	1.39	4.85	4.47	3.93
fus0012	271	65	32,340	3893	7710	1033	878	747	63	63	62	61	97	97	95	94	0.82	6.10	7.06	8.17
fus0013	741	135	33,768	4580	6133	800	692	604	124	67	62	57	92	50	46	42	2.02	8.38	8.96	9.44
fus0015	653	156	36,970	4344	8814	867	562	364	132 85	57	37	85	54	37	24	1.50	9.80	10.14	10.16	

b) Thalamic segmentation map to postcentral gyrus

	Lesion		TSM	VOL_O(mm^3)								(VOL_O/VOL_L)%					(VOL_O/VOL_TSM)%		
	V	VOL(mm^3)	V	MI	NT	30%	40%	50%	NT	30%	40%	50%	NT	30%	40%	50%	NT	30%	40%	50%
fus001	430	103	29,117	4653	6942	821	715	594	103	49	44	37	100	48	43	36	1.48	5.97	6.15	6.23
fus002	292	70	25,168	4236	6001	1133	947	737	21	21	20	18	30	30	29	26	0.35	1.85	2.11	2.44
fus004	667	121	28,759	4977	5223	845	723	640	108	67	61	56	89	55	50	46	2.07	7.93	8.44	8.75
fus005	565	103	43,104	4752	7828	979	845	732	101	84	80	74	98	82	78	72	1.29	8.58	9.47	10.11
fus006	686	125	37,460	4073	6803	1273	1091	941	77	75	70	65	62	60	56	52	1.13	5.89	6.42	6.91
fus008	528	126	29,454	4442	7022	841	728	628	126	79	71	62	100	63	56	49	1.79	9.39	9.75	9.87
fus009	377	90	32,905	4914	7845	1107	798	536	36	0	0	0	40	0	0	0	0.46	0.00	0.00	0.00
fus0010	694	126	38,599	4496	7010	811	621	471	80	41	32	25	63	33	25	20	1.14	5.06	5.15	5.31
fus0011	450	107	29,815	4207	7108	513	439	371	98	2	0	0	92	2	0	0	1.38	0.39	0.00	0.00
fus0012	271	65	34,176	4799	8148	1157	1039	946	63	39	36	34	97	60	55	52	0.77	3.37	3.46	3.59
fus0013	741	135	36,410	4630	6613	1129	1014	918	124	52	45	42	92	39	33	31	1.88	4.61	4.44	4.58
fus0015	653	156	37,020	4457	8826	1816	1546	1196	132	126	119	102	85	81	76	65	1.50	6.94	7.70	8.53

V = voxels, VOL = volume, VOL_O = volume of overlapping, MI = maximum intensity, NT = no threshold, TSM = thalamic segmentation map, VOL_L = volume of MRgFUS induced lesion, VOL_TSM = volume of thalamic segmentation.

the maximum intensity value was retrieved and then different percentages of the maximum intensity value (30%, 40% and 50%) were applied to threshold the thalamic segmentation maps. The volume of the thresholded maps was calculated and the overlapping (VOL_O) between the connectivity-based thalamic segmentation maps to both targets (pre-central and post-central gyrus) and lesion area was evaluated. Finally, we compared the overlapping volume (thresholded/unthresholded maps) with the MRgFUS induced lesion ((VOL_O/VOL_L) %) and the thalamic segmentation maps ((VOL_O/VOL_TSM) %).

3.3. Prediction of improved clinical outcome

The initial assessment between the volume of the lesion and the percentage of clinical improvement 1 month and 1 year after MRgFUS, did not demonstrate significant results between the two parameters (Supplementary material Fig. 1). The analysis of ROC curves showed that the volume of overlap between the lesion and the thalamic probabilistic maps can predict which patients had a superior clinical outcome after MRgFUS treatment. The area under the ROC curve was 0.80 (95% confidence interval:0.54–1; $p < 0.005$) when considering the overlap of the MRgFUS lesion with the thalamic probabilistic map to precentral gyrus using a 30% threshold and 0.76 (95% confidence interval: 0.48–1; $p < 0.005$) when considering the overlap with the thalamic probabilistic map to postcentral gyrus (at 30% threshold) (Fig. 4). Using other thresholds (or no threshold) for the probabilistic thalamic maps resulted in lower areas under the ROC curve (Fig. 4). When volume of intersection was normalized by the volume of lesion or thalamic segmentation map, low accuracy values were identified. Likewise, the value of the mean Euclidean distance between the lesions' voxels with the voxel with the maximum intensity value within thalamic segmentation map was low (Supplementary material Figs. 2, 3).

4. Discussion

Given inherent variability in brain anatomy across patients, we sought to evaluate a probabilistic tractography approach to predict outcomes and potentially target MRgFUS thalamotomy. In particular, we employ methods that are automated, are widely available, and do not require manual segmentation or user input to define seeds or masks, ensuring the method is practical and potentially adoptable. As hypothesized, we found that the percentage overlap between connectivity-based thalamic segmentation maps to the pre- and post-central gyri and the thalamic lesion predicted the improvement in clinical outcome. Patients with higher percentage of overlap between the lesion and the tractography-defined thalamic targets demonstrated superior response to MRgFUS treatment compared to other patients.

Consistent with previous literature mostly from DBS studies (Coenen et al., 2017, 2014, 2011; Fenoy and Schiess, 2017; Hyam et al., 2012; Kincses et al., 2012; Klein et al., 2012; Pouratian et al., 2011; Sammartino et al., 2016; Sasada et al., 2017), we report that better clinical outcome was associated with stronger structural connectivity to pre- and post-central gyri (including premotor cortex), brainstem and cerebellum compared to the connectivity of patients with inferior clinical outcomes (Fig. 2). The fewer tracts observed in the group with inferior outcomes is likely due to less consistency amongst this group relative to the consistency of tracts in those with superior outcomes.

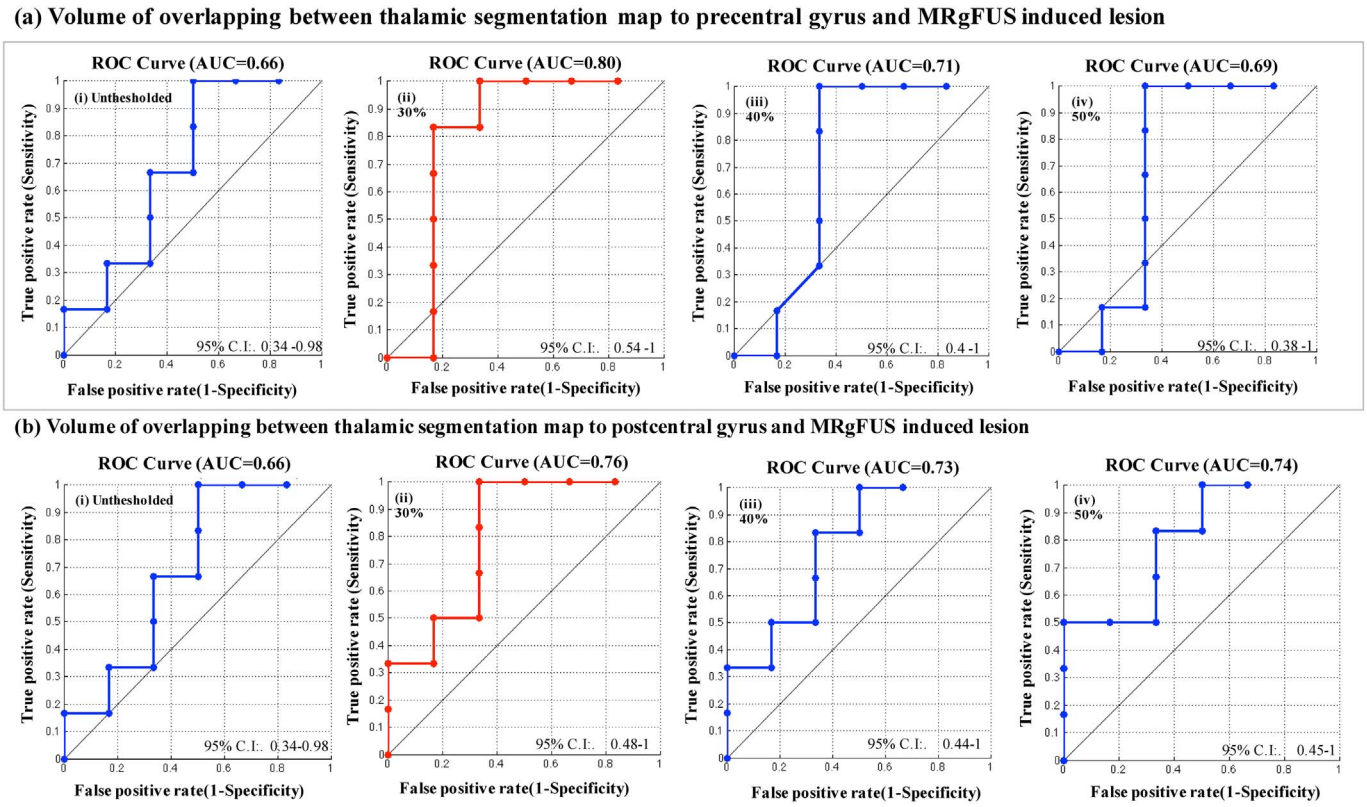

Fig. 4. Prediction of superior clinical outcome using the volume of overlapping between thalamic segmentation maps and MRgFUS induced lesion.
The volume of intersection between the MRgFUs treatment-induced lesion area and thalamic-segmentation maps to both targets precentral (a) and postcentral (b) gyrus ((unthresholded (i)/thresholded maps (ii–iv))) was used as feature to predict the superior clinical outcome. The area under the ROC curve was 0.80 (a-ii, red color) (95% confidence interval:0.54–1; $p < 0.005$) using as feature the overlapping of thalamic probabilistic map to motor target (at 30% threshold) and (b-ii, red color) 76% (95% confidence interval:0.48–1; $p < 0.005$) when as feature it was used the thalamic probabilistic map to sensory target (at 30% threshold).

Tractography results from lesion demonstrated the caudal projection to the cerebellum as a characteristic tract that confirms the role of Vim as the anatomically cerebellar receiving area of the thalamus. These results contribute to a better understanding of the underlying pathology and highlight the predictive power of lesion overlap with tractography-defined targets. Probabilistic tractography may therefore be an effective non-invasive imaging tool that can be used to overcome current imaging limitations, particularly when internal anatomy is not clearly evident on structural imaging (Nowinski et al., 2006, 2004; O'Gorman et al., 2011). While these results are intriguing, one must still consider that the observed differences in whole brain tractography may be due to technical issues and may not necessarily be treatment, outcome, or group-related.

In previous studies, probabilistic and deterministic approaches were used for thalamic targeting in ET patients (Pouratian et al., 2011, Kim et al., 2016, Hyam et al., 2012, Kincses et al., 2012,Sedrak et al., 2011). Pouratian et al. (2011) reported a new method of targeting patient-specific therapeutic thalamic target for the treatment of tremor based on individualized probabilistic tractography analysis of thalamic connectivity patterns to premotor and supplementary motor cortices. The same approach (Kim et al., 2016) was validated for the definition of Vim in a tremor-dominant Parkinson's disease patient. Others have used probabilistic tractography to explore the individual thalamic nuclei connectivity profiles and to reveal the inter-individual variability of the anatomical position of nuclei areas (Hyam et al., 2012; Kincses et al., 2012). In a number of recent studies (Sammartino et al., 2016, Fenoy and Schiess, 2017; Sasada et al., 2017), deterministic tractography has been used for targeting the thalamus for treatment of tremor. Interestingly, one approach is to use tractography to indirectly target the ViM, by delineating the pyramidal tract and medial lemniscus, and targeting 3 mm medial and anterior to these, respectively (Sammartino et al., 2016). In contrast to this empiric approach, our current results suggest that having the lesion overlap with thalamic regions with connectivity with the postcentral gyrus may play a therapeutic role. More direct targeting of the cerebello-thalamo-premotor cortical fiber tract have also been reported to identify the optimal target (Fenoy and Schiess, 2017; Sasada et al., 2017). Still, the AUC is not 100% for any of the comparisons, suggesting this is not a perfect methodology and highlighting that targeting and patient outcomes are multifactorial and cannot completely be accounted for by connectivity-based target estimation.

Still, there is a controversy in literature about which diffusion tractography analytic approach is more reliable for reproducing known anatomy, with results highly dependent on data quality, the algorithm selected, and the parameter settings (Knösche et al., 2015; Thomas et al., 2014). Deterministic tractography is a fast approach, but is characterized by increased uncertainty in dense areas where it cannot resolve crossing fibers and is prone to sampling limitations (Avecillas-Chasin et al., 2015). The probabilistic approach on the other hand is computationally demanding and time intensive compared to deterministic and it can be more sensitive to non-dominant fiber pathways and more prone to false positives (Behrens et al., 2007). However, its data-driven nature may provide a better practical approach in delineation of individualized anatomy over deterministic. Moreover, computational limitations are increasingly overcome with accelerated hardware platforms. Ultimately, a head-to-head comparison of deterministic vs probabilistic tractography algorithms will need to be done for each target and each application, but this is beyond the focus of the current work. Tractography constitutes the only non-invasive available tool for the evaluation of white-matter microstructure and to address the clinical need for white matter pathways characterization (Basser and Özarslan, 2014). Moreover, even if it is not reliable at precisely

reproducing known anatomy, these methods can still theoretically provide usable biomarkers to guide functional neurosurgery.

The main limitation of the current study is the small sample size of our population. MRgFUS thalamotomy for ET was an investigational approach and the available data were restricted. However, with the recent FDA approval, the clinical research will be rapidly expanded. We believe even if the available data are restricted, we have to optimize opportunities and make investigations that will contribute to the better understanding of the field. Further studies are needed with larger sample size population to assess improvements in treatment efficacy using tractography for preoperative Vim targeting and to explore the predictive value of probabilistic tractography guided thalamic targeting for ET patients. Also, the number of directions (20 directions) that was used in the current DTI acquisition protocol may be another limitation of the study since it can introduce uncertainty on the results. Larger number of directions lead to improved precision in the tracking results and a reduction in the spread of the results (Tournier et al., 2011).

5. Conclusion

Transcranial MRgFUS is a significant new development in functional neurosurgery field. Imaging analysis techniques like probabilistic tractography may potentially be used to increase the efficacy and consistency of outcomes with MRgFUS and potentially shorten treatment times by identifying optimal targets in advance of treatment. These methods may be applicable to other incisionless approaches for treatment of tremor, such as stereotactic radiosurgery. The current results provide further validation of this potentially useful methodology. Prospective evaluation, comparison with deterministic tractography, and development of appropriate clinical platforms are necessary prior to consideration of routine adoption in clinical practice.

Supplementary data to this article can be found online at https://doi.org/10.1016/j.nicl.2017.12.018.

Acknowledgements

This work has been supported by philanthropic support from the Casa Colina Centers for Rehabilitation.

References

Alusi, S.H., Aziz, T.Z., Glickman, S., Jahanshahi, M., Stein, J.F., Bain, P.G., 2001. Stereotactic lesional surgery for the treatment of tremor in multiple sclerosis: a prospective case-controlled study. Brain 124, 1576–1589. http://dx.doi.org/10.1093/brain/124.8.1576.

Andersson, J.L.R., Jenkinson, M., Smith, S., 2007. Non-linear registration, aka spatial normalisation. In: FMRIB Technical Report TR07JA2. vol. 22 Oxford Cent. Funct. Magn. Reson. Imaging Brain, Dep. Clin. Neurol. Oxford Univ., Oxford, UK.

Avecillas-Chasin, J.M., Alonso-Frech, F., Parras, O., del Prado, N., Barcia, J.A., 2015. Assessment of a method to determine deep brain stimulation targets using deterministic tractography in a navigation system. Neurosurg. Rev. 38, 739–751. http://dx.doi.org/10.1007/s10143-015-0643-1.

Basser, P.J., Özarslan, E., 2014. Chapter 1 - Introduction to Diffusion MR BT - Diffusion MRI, second edition. Academic Press, San Diego, pp. 3–9. http://dx.doi.org/10.1016/B978-0-12-396460-1.00001-9.

Behrens, T.E.J., Woolrich, M.W., Jenkinson, M., Johansen-Berg, H., Nunes, R.G., Clare, S., Matthews, P.M., Brady, J.M., Smith, S.M., 2003a. Characterization and propagation of uncertainty in diffusion-weighted MR imaging. Magn. Reson. Med. 50, 1077–1088. http://dx.doi.org/10.1002/mrm.10609.

Behrens, T.E.J, Johansen-Berg, H., Woolrich, M.W., Smith, S.M., Wheeler-Kingshott, C.A., Boulby, P.A., Barker, G.J., Sillery, E.L., Sheehan, K., Ciccarelli, O., Thompson, A.J., Brady, J.M., Matthews, P.M., 2003b. Non-invasive mapping of connections between human thalamus and cortex using diffusion imaging. Nat. Neurosci. 6, 750–757. http://dx.doi.org/10.1227/01.NEU.0000309595.77090.89.

Behrens, T.E.J., Berg, H.J., Jbabdi, S., Rushworth, M.F., W., M., 2007. Probabilistic diffusion tractography with multiple fibre orientations: what can we gain? NeuroImage 34, 144–155. http://dx.doi.org/10.1016/j.neuroimage.2006.09.018.

Bittar, R.G., Hyam, J., Nandi, D., Wang, S., Liu, X., Joint, C., Bain, P.G., Gregory, R., Stein, J., Aziz, T.Z., 2005. Thalamotomy versus thalamic stimulation for multiple sclerosis tremor. J. Clin. Neurosci. 12, 638–642. http://dx.doi.org/10.1016/j.jocn.2004.09.008.

Brittain, J.-S., Cagnan, H., Mehta, A.R., Saifee, T.A., Edwards, M.J., Brown, P., 2015. Distinguishing the central drive to tremor in Parkinson's disease and essential tremor. J. Neurosci. 35, 795–806. http://dx.doi.org/10.1523/JNEUROSCI.3768-14.2015.

Chandran, V., Pal, P.K., 2013. Quality of life and its determinants in essential tremor. Parkinsonism Relat. Disord. 19, 62–65. http://dx.doi.org/10.1016/j.parkreldis.2012.06.011.

Coenen, V.A., Allert, N., Mädler, B., 2011. A role of diffusion tensor imaging fiber tracking in deep brain stimulation surgery: DBS of the dentato-rubro-thalamic tract (drt) for the treatment of therapy-refractory tremor. Acta Neurochir. 153, 1579–1585. http://dx.doi.org/10.1007/s00701-011-1036-z.

Coenen, V.A., Allert, N., Paus, S., Kronenbürger, M., Urbach, H., Mädler, B., 2014. Modulation of the Cerebello-Thalamo-Cortical network in thalamic deep brain stimulation for tremor: a diffusion tensor imaging study. Neurosurgery 75, 657–669. http://dx.doi.org/10.1227/NEU.0000000000000540.

Coenen, V.A., Varkuti, B., Parpaley, Y., Skodda, S., Prokop, T., Urbach, H., Li, M., Reinacher, P.C., 2017. Postoperative neuroimaging analysis of DRT deep brain stimulation revision surgery for complicated essential tremor. Acta Neurochir. 159, 779–787. http://dx.doi.org/10.1007/s00701-017-3134-z.

Dormont, D., Cornu, P., Pidoux, B., Bonnet, A.M., Biondi, A., Oppenheim, C., Hasboun, D., Damier, P., Cuchet, E., Philippon, J., Agid, Y., Marsault, C., 1997. Chronic thalamic stimulation with three-dimensional MR stereotactic guidance. Am. J. Neuroradiol. 18, 1093–1107.

Elias, W.J., Shah, B.B., 2014. Tremor. JAMA 311, 948. http://dx.doi.org/10.1001/jama.2014.1397.

Elias, W.J., Huss, D., Voss, T., Loomba, J., Khaled, M., Zadicario, E., Frysinger, R.C., Sperling, S.A., Wylie, S., Monteith, S.J., Druzgal, J., Shah, B.B., Harrison, M., Wintermark, M., 2013. A pilot study of focused ultrasound thalamotomy for essential tremor. N. Engl. J. Med. 369, 640–648. http://dx.doi.org/10.1056/NEJMoa1300962.

Elias, W.J., Lipsman, N., Ondo, W.G., Ghanouni, P., Kim, Y.G., Lee, W., Schwartz, M., Hynynen, K., Lozano, A.M., Shah, B.B., Huss, D., Dallapiazza, R.F., Gwinn, R., Witt, J., Ro, S., Eisenberg, H.M., Fishman, P.S., Gandhi, D., Halpern, C.H., Chuang, R., Butts Pauly, K., Tierney, T.S., Hayes, M.T., Cosgrove, G.R., Yamaguchi, T., Abe, K., Taira, T., Chang, J.W., 2016. A randomized trial of focused ultrasound thalamotomy for essential tremor. N. Engl. J. Med. 375, 730–739. http://dx.doi.org/10.1056/NEJMoa1600159.

Fang, W., Chen, H., Wang, H., Zhang, H., Puneet, M., Liu, M., Lv, F., Luo, T., Cheng, O., Wang, X., Lu, X., 2016. Essential tremor is associated with disruption of functional connectivity in the ventral intermediate nucleus-motor cortex-cerebellum circuit. Hum. Brain Mapp. 37, 165–178. http://dx.doi.org/10.1002/hbm.23024.

Fenoy, A.J., Schiess, M.C., 2017. Deep brain stimulation of the Dentato-Rubro-Thalamic tract: outcomes of direct targeting for tremor. Neuromodulation 2017. http://dx.doi.org/10.1111/ner.12585.

Hyam, J.A., Owen, S.L.F., Kringelbach, M.L., Jenkinson, N., Stein, J.F., Green, A.L., Aziz, T.Z., 2012. Contrasting connectivity of the ventralis intermedius and ventralis oralis posterior nuclei of the motor thalamus demonstrated by probabilistic tractography. Neurosurgery 70, 162–169. http://dx.doi.org/10.1227/NEU.0b013e3182262c9a.

Ilinsky, I.A., Kultas-Ilinsky, K., 2002. Motor thalamic circuits in primates with emphasis on the area targeted in treatment of movement disorders. Mov. Disord. 17. http://dx.doi.org/10.1002/mds.10137.

Jenkinson, M., Bannister, P., Brady, M., Smith, S., 2002. Improved optimization for the robust and accurate linear registration and motion correction of brain images. NeuroImage 17, 825–841. http://dx.doi.org/10.1006/nimg.2002.1132.

Kim, W., Chivukula, S., Hauptman, J., Pouratian, N., 2016. Diffusion tensor imaging-based thalamic segmentation in deep brain stimulation for chronic pain conditions. Stereotact. Funct. Neurosurg. 94, 225–234.

Kim, W., Sharim, J., Tenn, S., Kaprealian, T., Bordelon, Y., Agazaryan, N., Pouratian, N., 2017. Diffusion tractography imaging–guided frameless linear accelerator stereotactic radiosurgical thalamotomy for tremor: case report. J. Neurosurg. 1–7. http://dx.doi.org/10.3171/2016.10.JNS161603.

Kincses, Z.T., Szabó, N., Valálik, I., Kopniczky, Z., Dézsi, L., Klivényi, P., Jenkinson, M., Király, A., Babos, M., Vörös, E., Barzó, P., Vécsei, L., 2012. Target identification for stereotactic thalamotomy using diffusion tractography. PLoS One 7. http://dx.doi.org/10.1371/journal.pone.0029969.

Klein, J.C., Barbe, M.T., Seifried, C., Baudrexel, S., Runge, M., Maarouf, M., Gasser, T., Hattingen, E., Liebig, T., Deichmann, R., Timmermann, L., Weise, L., Hilker, R., 2012. The tremor network targeted by successful VIM deep brain stimulation in humans. Neurology 78, 787–795. http://dx.doi.org/10.1212/WNL.0b013e318249f702.

Knösche, T.R., Anwander, A., Liptrot, M., Dyrby, T.B., 2015. Validation of tractography: comparison with manganese tracing. Hum. Brain Mapp. 36, 4116–4134. http://dx.doi.org/10.1002/hbm.22902.

Li, S.C.S.B., et al., W.C.C, 1985. A prevalence survey of Parkinson's disease and other movement disorders in the People's Republic of China. Arch. Neurol. 42, 655–657.

Lipsman, N., Schwartz, M.L., Huang, Y., Lee, L., Sankar, T., Chapman, M., Hynynen, K., Lozano, A.M., 2013. MR-guided focused ultrasound thalamotomy for essential tremor: a proof-of-concept study. Lancet Neurol. 12, 462–468. http://dx.doi.org/10.1016/S1474-4422(13)70048-6.

Louis, E.D., 2014. Re-thinking the biology of essential tremor: from models to morphology. Parkinsonism Relat. Disord. 20, S88–S93. http://dx.doi.org/10.1016/S1353-8020(13)70023-3.

Louis, E.D., Ferreira, J.J., 2010. How common is the most common adult movement disorder? Update on the worldwide prevalence of essential tremor. Mov. Disord. 25, 534–541. http://dx.doi.org/10.1002/mds.22838.

Louis, E.D., Ottman, R., Hauser, a, 1998. How common is the most common adult movement disorder? Estimates of the prevalence of essential tremor throughout the world. Mov. Disord. 13, 5–10.

Nowinski, W.L., Belov, D., Pollak, P., Benabid, A.L., 2004. A probabilistic functional atlas of the human subthalamic nucleus. Neuroinformatics 2, 381–398. http://dx.doi.org/10.1385/NI:2:4:381.

Nowinski, W.L., Belov, D., Thirunavuukarasuu, A., Benabid, A.L., 2006. A probabilistic functional atlas of the VIM nucleus constructed from pre-, intra- and postoperative electrophysiological and neuroimaging data acquired during the surgical treatment of Parkinson's disease patients. Stereotact. Funct. Neurosurg. 83, 190–196. http://dx.doi.org/10.1159/000091082.

O'Gorman, R.L., Shmueli, K., Ashkan, K., Samuel, M., Lythgoe, D.J., Shahidiani, A., Wastling, S.J., Footman, M., Selway, R.P., Jarosz, J., 2011. Optimal MRI methods for direct stereotactic targeting of the subthalamic nucleus and globus pallidus. Eur. Radiol. 21, 130–136. http://dx.doi.org/10.1007/s00330-010-1885-5.

Papavassiliou, E., Rau, G., Heath, S., Abosch, A., Barbaro, N.M., Larson, P.S., Lamborn, K., Starr, P.A., Sharan, A.D., Rezai, A.R., Benabid, A.L., Lozano, A.M., 2004. Thalamic deep brain stimulation for essential tremor: relation of lead location to outcome. Neurosurgery 54, 1120–1130. http://dx.doi.org/10.1227/01.NEU.0000119329.66931.9E.

Park, S.H., Goo, J.M., Jo, C.-H., 2004. Receiver operating characteristic (ROC) curve: practical review for radiologists. Korean J. Radiol. 5, 11–18. http://dx.doi.org/10.3348/kjr.2004.5.1.11.

Pouratian, N., Zheng, Z., Bari, A.A., Behnke, E., Elias, W.J., DeSalles, A.A.F., 2011. Multi-institutional evaluation of deep brain stimulation targeting using probabilistic connectivity-based thalamic segmentation. J. Neurosurg. 115, 995–1004. http://dx.doi.org/10.3171/2011.7.JNS11250.

Raethjen, J., Deuschl, G., 2012. The oscillating central network of essential tremor. Clin. Neurophysiol. 123, 61–64. http://dx.doi.org/10.1016/j.clinph.2011.09.024.

Sammartino, F., Krishna, V., King, N.K.K., Lozano, A.M., Schwartz, M.L., Huang, Y., Hodaie, M., 2016. Tractography-based ventral intermediate nucleus targeting: novel methodology and intraoperative validation. Mov. Disord. 31, 1217–1225. http://dx.doi.org/10.1002/mds.26633.

Sasada, S., Agari, T., Sasaki, T., Kondo, A., Shinko, A., Wakamori, T., Okazaki, M., Kin, I., Kuwahara, K., Kameda, M., Yasuhara, T., Date, I., 2017. Efficacy of fiber tractography in the stereotactic surgery of the thalamus for patients with essential tremor. Neurol. Med. Chir. (Tokyo). http://dx.doi.org/10.2176/nmc.oa.2016-0277. (oa.2016-0277).

Sedrak, M., Gorgulho, A., Frew, A., Behnke, E., DeSalles, A., Pouratian, N., 2011. Diffusion tensor imaging and colored fractional anisotropy mapping of the ventralis intermedius nucleus of the thalamus. Neurosurgery 69, 1124–1130. http://dx.doi.org/10.1227/NEU.0b013e3182296a42.

Smith, S.M., 2002. Fast robust automated brain extraction. Hum. Brain Mapp. 17, 143–155. http://dx.doi.org/10.1002/hbm.10062.

Stacy, M.A., Elble, R.J., Ondo, W.G., Wu, S.C., Hulihan, J., 2007. Assessment of interrater and intrarater reliability of the Fahn-Tolosa-Marin Tremor Rating Scale in essential tremor. Mov. Disord. 22, 833–838. http://dx.doi.org/10.1002/mds.21412.

Thomas, C., Ye, F.Q., Irfanoglu, M.O., Modi, P., Saleem, K.S., Leopold, D.A., Pierpaoli, C., 2014. Anatomical accuracy of brain connections derived from diffusion MRI tractography is inherently limited. Proc. Natl. Acad. Sci. 111, 16574–16579. http://dx.doi.org/10.1073/pnas.1405672111.

Tournier, J., Mori, S., Leemans, a, 2011. Diffusion Tensor Imaging and Beyond. Magn. Reson. 65, 1532–1556. http://dx.doi.org/10.1002/mrm.22924.Diffusion.

Wintermark, M., Druzgal, J., Huss, D.S., Khaled, M.A., Monteith, S., Raghavan, P., Huerta, T., Schweickert, L.C., Burkholder, B., Loomba, J.J., Zadicario, E., Qiao, Y., Shah, B., Snell, J., Eames, M., Frysinger, R., Kassell, N., Elias, W.J., 2014. Imaging findings in MR imaging-guided focused ultrasound treatment for patients with essential tremor. AJNR Am. J. Neuroradiol. 35, 891–896. http://dx.doi.org/10.3174/ajnr.A3808.